HHS Public Access

Author manuscript

Magn Reson Med. Author manuscript; available in PMC 2019 May 01.

Published in final edited form as:

Magn Reson Med. 2018 May ; 79(5): 2745–2751. doi:10.1002/mrm.26918.

Validation of Highly-Accelerated Real-Time Cardiac Cine MRI with Radial k-space Sampling and Compressed Sensing in Patients at 1.5T and 3T

Hassan Haji-Valizadeh, MS[1,2], **Amir A. Rahsepar, MD**[2], **Jeremy D. Collins, MD**[2], **Elwin Bassett, BS**[4], **Tamara Isakova, MD**[3], **Tobias Block, PhD**[5], **Ganesh Adluru, PhD**[6], **Edward VR DiBella, PhD**[6], **Daniel C. Lee, MD**[2,7], **James Carr, MD**[2], **Daniel Kim, PhD**[2], and **The CKD Optimal Management with Binders and NicotinamidE (COMBINE) Study Group**

[1]Biomedical Engineering, Northwestern University, Evanston, Illinois, United States

[2]Department of Radiology, Northwestern University, Chicago, Illinois, United States

[3]Division of Nephrology, Internal Medicine, Northwestern University, Chicago, Illinois, United States

[4]Physics Department, University of Utah, Salt Lake City, Utah, United States

[5]Department of Radiology, New York University, New York, New York, United States

[6]Department of Radiology and Imaging Science, University of Utah, Salt Lake City, Utah, United States

[7]Division of Cardiology, Internal Medicine, Northwestern University, Chicago, Illinois, United States

Abstract

Purpose—To validate an optimal 12-fold accelerated real-time cine MRI pulse sequence with radial k-space sampling and compressed sensing (CS) in patients at 1.5T and 3T.

Methods—We used two strategies to reduce image artifacts arising from gradient delays and eddy currents in radial k-space sampling with balanced steady-state free precession readout. We validated this pulse sequence against a standard breath-hold cine sequence in two patient cohorts – myocardial infarction (N=16) group at 1.5T and chronic kidney disease group (N=18) at 3T. Two readers independently performed visual analysis of 68 cine sets in four categories (myocardial definition, temporal fidelity, artifact, noise) on a 5-point Likert scale (1 = nondiagnostic, 2 = poor, 3 = adequate or moderate, 4 = good, 5 = excellent). Another reader calculated left ventricular (LV) functional parameters, including ejection fraction.

Results—Compared with standard cine, real-time cine produced non-significantly different visually assessed scores, except for the following categories: (i) temporal fidelity scores were significantly lower (P=0.013) for real-time cine at both field strengths, (ii) artifacts scores were significantly higher (P=0.013) for real-time cine at both field strengths, and (iii) noise scores were

Please send correspondence to: Daniel Kim, PhD, Department of Radiology, Northwestern University, 737 N. Michigan Avenue Suite 1600, Chicago, IL 60611, daniel.kim3@northwestern.edu, O:312.926.1733, F:312.926.5991.

significantly (P=0.013) higher for real-time cine at 1.5T. Standard and real-time cine pulse sequences produced LV functional parameters which were in good agreement (e.g., absolute mean difference in ejection fraction < 4%).

Conclusion—This study demonstrates that an optimal 12-fold accelerated, real-time cine MRI pulse sequence using radial k-space sampling and CS produces good-to-excellent visual scores and relatively accurate LV functional parameters in patients at 1.5T and 3T.

Keywords

Compressed sensing; radial k-space; Cartesian k-space; real-time cine MRI; tiny golden angles; cardiac function

Introduction

While ECG-gated, breath-hold cine MRI with balanced steady-state free precession (b-SSFP)(1) readout is considered the gold standard test for evaluation of cardiac function (2), it has several limitations, including long scan time and sensitivity to irregular heart rhythm and breathing motion. Thus, standard cine MRI often produces poor image quality in patients with dyspnea (e.g., heart failure, critically ill) and/or arrhythmia (e.g., atrial fibrillation).

One approach to address these limitations of standard cine MRI is to perform real-time cine MRI (3) during free breathing. However, commercial real-time cine MRI acquisitions using dynamic parallel imaging typically yield low spatio-temporal resolution (4, 5) due to their slow imaging speed (e.g., acceleration factor 3). More advanced investigational acceleration methods that could be used include partially separable functions (6), k-t SENSE (7), through-time GRAPPA (8, 9), and compressed sensing (CS) (10–13), with different methods having advantages (e.g., net acceleration rate) and disadvantages (e.g., image reconstruction time, prior information such as a pre-scan). In this work, we focus our investigation on CS because of its ability to achieve high acceleration rates, typically 8 or higher.

This study builds on a prior study which reported that radial k-space sampling produces better results than Cartesian k-space sampling in real-time cine MRI with b-SSFP readout (14), and another prior study which reported that CS or regularized nonlinear inversion reconstruction can be used to highly-accelerate real-time cine MRI with radial k-space sampling and achieve a high temporal resolution on the order of 40 ms (12). An even higher temporal resolution may be needed for imaging pediatric patients, patients with tachycardia (heart rate > 100 beats per minute), or patient during stress testing. In this study, we sought to further optimize real-time cine MRI with radial k-space sampling and CS by incorporating several improvements to: (i) achieve higher temporal resolution (~30 ms), (ii) enable retrospective binning to select optimal temporal resolution, and (iii) reduce image artifacts associated with gradient delays and eddy currents. As an important first step towards clinical applications, we sought to validate an optimized, highly-accelerated, real-time cine MRI pulse sequence with radial k-space sampling and CS in adult patients at both 1.5T and 3T, which is important since a major gap in highly-accelerated cardiovascular MRI methods with CS is the lack of validation studies in patients with disease (15).

Methods

Theoretical Considerations for the Optimization of Methods

As per Wundrak et al.(16), we used the 7th Fibonacci sequence of golden angles, which is equal to 23.62814°, to reduce eddy currents associated with k-space jumps in b-SSFP readout (14, 16, 17). For brevity, we refer to it as tiny golden angle (TGA)(18, 19) throughout.

Using the imaging parameters proposed by Voit et al. (12) as a guide, we elected to develop a protocol with spatial resolution on the order of 2.0 mm × 2.0 mm and temporal resolution on the order of 40 ms or better. To identify the acceptable limits of acceleration, we acquired a fully sampled ECG-gated breath-hold cine MRI data (image acquisition matrix = 144 × 144, TR = 2.7 ms) from a male patient (age = 63 years), retrospectively undersampled the k-space using a tiny golden angle (TGA)(18, 19), and found that acceleration factor (R) greater than or equal to 12 (i.e., 12 k-space lines per image, temporal resolution = 32 ms) produces high data fidelity as defined as structural similarity index (SSIM)(20) greater than or equal to 0.95 (see Figure S1 in Supporting Information).

Radial k-space acquisition is sensitive to magnetic field gradient delays and eddy currents. This problem can be solved by acquiring k-space trajectory calibration data (21). In this study, we designed the pulse sequence to acquire calibration data without incurring a time penalty by replacing post-scan, dummy scans with calibration scans, as shown in Figure 1. Another interesting aspect of radial k-space sampling is whether the angular sequence should rotate over 360° or 180°, since both strategies have identical sampling patterns in k-space. As shown in Supporting Figure S2, for the 360° rotation case, there are four groups of echoes in terms of spatial encoding gradient polarities. For the 180° rotation case, only two groups of echoes are present, but there is a slight increase in eddy currents. As shown in Figure S3, when TGA = 23.62814°, 12 rays acquired per image, and temporal total variation (TTV) is the constraint in CS reconstruction, rotating over 180° produced less aliasing artifacts than over 360° with or without phase correction (see corresponding movie files in Supporting Information for dynamic display of residual signal and phase). As such, we used TGA sampling over 180° with phase correction throughout this study.

Patients

This study was conducted by leveraging two ongoing MRI studies which included standard cine MRI in parent protocols. The first ongoing study comprised of patients with prior history of myocardial infarction (MI)(mean age = 59.4 ± 12.9 years; 9 males and 7 females; mean heart rate = 65.7 ± 9.1 bpm; left ventricular ejection fraction ranging from 29 – 73%), whereas the second ongoing study comprised of patients with chronic kidney disease (CKD) (mean age = 62.4 ± 16.2 years; 7 males and 11 females; mean heart rate = 65.3 ± 7.2 bpm; left ventricular ejection fraction ranging from 46 – 78%). A detailed list of clinical profiles is not relevant for this study and is thus omitted due to space constraint. Human imaging was conducted in accordance with protocols approved by our institutional Review Board; all subjects provided written informed consent.

MRI Hardware

The first cohort of MI patients were scanned on a 1.5T whole-body MRI scanner (Aera, Siemens Healthcare, Erlangen, Germany), whereas the second cohort of CKD patients were scanned on a 3T whole-body MRI scanner (Skyra, Siemens Healthcare, Erlangen, Germany). Both scanners were equipped with a gradient system capable of achieving a maximum gradient strength of 45 mT/m and a slew rate of 200 T/m/s. The RF excitation on both scanners was performed using the body coil. Standard multi-coil arrays (anterior and spine elements, typically 12–15 elements total) were employed for signal reception.

Pulse Sequence

Relevant imaging parameters for standard breath-hold cine MRI at 1.5T included: field of view (FOV) in the frequency-encoding direction ranging from 340 mm to 500 mm, 81.2% FOV in the phase-encoding direction, image acquisition matrix = 192 × 133, R = 1.7 with GRAPPA (22), slice thickness = 6 mm, slice gap = 4 mm, flip angles ranging from 58°–70°, receiver bandwidth = 930 Hz/pixel, TE = 1.2 ms, TR = 2.7 ms, acquired k-space lines per frame = 13, temporal resolution = 35 ms (interpolated to 25 cardiac frames with retrospective ECG gating), scan duration = 7 heart beats (1 heart beat for dummy scan), and number of slices varying from 9 to 12 depending on patient's heart size. Standard cine MRI at 3T used the same imaging parameters, except: FOV in the frequency-encoding direction ranging from 360 mm to 420 mm, 100% FOV in the phase-encoding direction, image acquisition matrix = 192 × 192, R = 1.8, slice thickness = 8 mm, slice gap = 0 mm, flip angles ranging from 38°–46°, TE = 1.1 ms, TR = 2.5 ms, acquired k-space lines per frame = 15, temporal resolution = 38 ms (interpolated to 25 cardiac frames with retrospective ECG gating), scan duration = 13 heart beats (1 heart beat for dummy scan), and receiver bandwidth = 1445 Hz/pixel. Some differences between 1.5T and 3T protocols were unavoidable because our study was ancillary to two different parent studies.

Real-time cine with radial CS used the following set of imaging parameters at both 1.5T and 3T, including: FOV = 300 × 300 mm, image acquisition matrix = 144 × 144, slice thickness = 8 mm, slice gap = 0 mm, TE = 1.3 ms, TR = 2.7 ms, receiver bandwidth = 990 Hz/pixel, temporal resolution ranging = 32 ms, number of slices = 14, tiny golden angles = 23.62814°, flip angles ranged from 60–80° at 1.5T and 40°–50° at 3T, and number of cardiac phases = 46. The scan time for 2D plane was 3 heart beats (1 heart beat for pre-scan dummy scan, next two heart beats for data scan, calibration scan, and post-scan dummy scan, as shown in Figure 1), and the total scan time for 14 slices was 42 continuous heart beats during free breathing. For trajectory calibration scan, we acquired 48 rays per slice (a pair with opposite polarities per angle; 7.5° angular steps).

Image reconstruction

Trajectory correction was performed as a pre-processing step, as previously described (21). Undersampled data were reconstructed using the GRASP framework (23) (radial k-t SPARSE-SENSE) and TTV with normalized regularization weight of 0.02. This regularization weight was determined empirically using the same approach as previously described (10). We used nonuniform fast Fourier transform (NUFFT) to minimize spatial blurring during the gridding process (24). CS reconstructions were performed offline in

MATLAB (Mathworks, Natick, MA, USA) running on Windows 7 Professional 64-bit platform (Microsoft Corporation, Redmond, WA, USA).

Visual Assessment

One radiologist (JDC) with 11 years and one cardiologist (DCL) with 15 years of clinical experience in reading cardiovascular MRI, respectively, performed visual assessment of diagnostic quality of cine data sets. For efficient analysis, evaluation was limited to 3 short-axis planes (base, mid, apex) only. In total, 68 cine data sets, grouped as a set of 3 short-axis planes, were randomized and de-identified for dynamic display. Prior to visual evaluation, the two readers were given training data sets to calibrating their scores together, where a score of 3 is defined as clinically usable. Following training, each reader was blinded to image acquisition type (standard cine and real-time with radial CS), each other, and clinical history. Each short-axis stack was graded on a 5-point Likert scale: conspicuity of myocardial border (1 = nondiagnostic, 2 = poor, 3 = adequate, 4 = good, 5 = excellent), temporal fidelity (or blurring) of wall motion (1 = nondiagnostic, 2 = poor, 3 = adequate, 4 = good, 5 = excellent), artifact level (1 = nondiagnostic, 2 = severe, 3 = moderate, 4 = mild, 5 = minimal), and apparent noise level (1 = nondiagnostic, 2 = severe, 3 = moderate, 4 = mild, 5 = minimal).

LV Function Assessment

In total, 68 cine data sets were analyzed by another reader (AAR) with 5 years of experience as a medical research fellow, using standard methods on a workstation equipped with the QMass7.2 software (Medis, Leiden, The Netherlands). Functional parameters included left ventricular (LV) ejection fraction (LVEF), end-systolic volume (ESV), end-diastolic volume (EDV), and stroke volume (SV), and LV mass. For consistency, the most basal slice was defined as the plane which has ≥ 50% of the blood pool surrounded by myocardium, and the most apical slice was defined as the plane showing blood pool at end diastole. Papillary muscles were excluded for the calculation of LV mass measurements.

Statistical Analysis

For comparing visual scores (conspicuity of myocardial border, temporal fidelity, artifacts, noise) between 2 groups (standard cine MRI and real-time cine), scores were initially averaged over 2 readers, and the mean scores were compared using the Wilcoxon Rank-Sum test. In addition to a priori comparisons, a post-hoc Bonferroni correction was made to account for multiple comparisons. The agreements in LV functional parameters between standard and real-time cine scans were calculated using the Bland-Altman analysis. All statistical analyses were performed using the Analyse-it software (Analyse-it Ltd., Leeds, United Kingdom).

Results

Figure 2 shows representative multi-slice images of a patient with prior MI obtained at 1.5T (see corresponding movie files in Supporting Information). Figure 3 shows corresponding images of a patient with CKD obtained at 3T (see corresponding movie files in Supporting Information). In both cases, real-time cine with radial CS produced results that approximate

standard cine MRI. Summarizing the results over 34 patients (see Table 1), compared with standard cine, real-time cine produced non-significantly different visually assessed scores, except for the following categories: (i) temporal fidelity scores were significantly lower (P=0.013) for real-time cine at both field strengths, (ii) artifacts scores were significantly higher (P=0.013) for real-time cine at both field strengths, and (iii) noise scores were significantly (P=0.013) higher for real-time cine at 1.5T. Note that for all four categories, mean scores were greater than 3.0, suggesting that all scores were deemed clinically usable by our readers.

As shown in Figure 4, the mean difference in LV ejection fraction was −3.0 and −1.6% for 1.5T and 3T, respectively, which correspond to −5.3 and −2.6% error relative to mean LV ejection fraction values 57.9 and 63.2 % at 1.5T and 3T, respectively. See Figure S4 in Supporting Information for agreement in EDV, ESV, SV, and LV mass.

Discussion

This study describes several improvements made to a prior work (12) on accelerated real-time cine MRI using radial k-space sampling and CS. We identified two strategies to reduce image artifacts arising from gradient delays and eddy currents in radial k-space sampling with b-SSFP. Consistent with a prior study at 1.5T (12), findings from this study show that 12-fold accelerated, real-time cine MRI with radial k-space sampling and CS produces good to excellent visual scores and relatively accurate LV functional parameters in patients at 1.5T and 3T.

The proposed 12-fold accelerated, real-time cine MRI using radial k-space sampling and CS has several advantages over previously reported real-time cine with radial k-space sampling and regularized nonlinear inversion reconstruction (12). First, the proposed method reports a 20% improvement in temporal resolution than prior work. This improvement may be important for imaging pediatric patients, patients with tachycardia (heart rate > 100 beats per minute), and patient during stress testing. Second, the use of a TGA sequence in the proposed method enables retrospective binning to select optimal temporal resolution, whereas prior work is incapable of rebinning because it used regularly spaced angles. Third, a combined use of trajectory correction and TGA sampling over 180° rotation reduced image artifacts arising from gradient delays and eddy currents. Compared with another real-time cine pulse sequence using a radial FLASH readout with 2 mm × 2 mm spatial resolution and 30 ms temporal resolution by Uecker et al. (25), our work produced similar spatial resolution (2.1 mm × 2.1 mm) and temporal resolution (32 ms) but higher contrast to noise ratio owing to b-SSFP readout.

This study includes several limitations. First, this study did not directly compare the performance between the proposed method and prior work (12). This is a common problem when comparing investigational methods that are unavailable. Second, there were both physiologic and parameter variations between cine scans. Standard cine scans were performed with breath-holding at both field strengths and a 4 mm gap between slices at 1.5T, whereas real-time cine scans were performed during free breathing without any gap between slices. Additional differences between cine scans that are noteworthy include:

prospective gating vs. retrospective gating and resolution differences. These variations could lead to a systematic difference in LV functional parameters. In this study, both EDV and ESV differences were relatively large. One solution to minimize this discrepancy is to perform real-time cine MRI with breath holding and match the spatial gap between slices. Regrettably, this study did not account for these effects. Third, this study did not evaluate intra- and inter-observer agreement of LV functional parameters of 68 cine sets, which was beyond the scope of this study. A future study is warranted to evaluate observer agreements of LV functional parameters. Fourth, the proposed R=12 was not fully vetted during this study. Further work may be needed to determine whether R=12 is applicable for different clinical contexts.

Rapid real-time cine MRI with high spatio-temporal resolution has numerous advantages over standard cine MRI. First, it can be used to drastically reduce the scan time from approximately 8–10 minutes with multiple breath-holds to continuous scanning over 42 heart beats during free breathing. Second, radial k-space sampling with irrational angles such as TGA allows retrospective rebinning of data to determine an optimal temporal resolution. This has an important practical benefit, because there is no need to repeat scanning if the initial scan was deemed to have poor temporal resolution, which would be the case for standard cine MRI. Third, it can be used to image patients with arrhythmia, which is a major source of image artifacts with standard cine MRI. Fourth, it can be used to image pediatric patients and provide a means to relax the need for general anesthesia. Fifth, it can be used to image patients with dyspnea or who are critically ill, since those patients may be unable to perform complete breath holding.

Rapid real-time cine MRI has disadvantages as well. First, as a prospectively gated scan, its images are not displayed in a standard retrospectively gated format. As such, during image analysis of LV function, user defined end-diastolic and end-systolic frames of all slices may not line up at the same time points. This issue can be resolved in the image processing software (QMass7.2 software; Medis, Leiden, The Netherlands) using the following process, but at the expense of increased time and complexity in image analysis. Step 1, draw myocardial contours on actual end-diastolic and systolic frames for all slices. Step 2, copy and paste diastolic and systolic contours onto two arbitrarily defined time points such that the two sets of contours line up in time. Step 3, calculate LV functional parameters. Note, this problem is common to all prospectively gated real-time cine MRI pulse sequences. One solution to overcome this problem is to perform a retrospective reconstruction of repeated real-time cine acquisitions (26), at the expense of increased scan time (16–20 s per slice) and sensitivity to arrhythmia. A retrospectively gated image reconstruction may be important for improving clinical workflow. A future work is warranted to directly compare the proposed real-time cine MRI to a retrospectively gated real-time cine (26).

In summary, this study describes an optimal 12-fold accelerated, real-time cine MRI pulse sequence with radial k-space sampling and CS and its validation in patients at 1.5T and 3T. Future work includes a study aimed to evaluating the clinical utility of highly-accelerated real-time cine with radial CS in challenging contexts such as atrial fibrillation, pediatrics, or heart failure.

Supplementary Material

Refer to Web version on PubMed Central for supplementary material.

Acknowledgments

Grant Support: This work was supported in part by funding from the National Institutes of Health (R01HL116895, R01HL138578, R21EB024315, R21AG055954, R01DK102438).

The authors thank funding support from the National Institutes of Health (R01HL116895, R01HL138578, R21EB024315, R21AG055954, R01DK102438). The authors thank Dr. Ann Ragin for her support in statistical analysis.

References

1. Carr JC, Simonetti O, Bundy J, Li D, Pereles S, Finn JP. Cine MR angiography of the heart with segmented true fast imaging with steady-state precession. Radiology. 2001; 219(3):828–34. [PubMed: 11376278]
2. Hundley WG, Bluemke DA, Finn JP, Flamm SD, Fogel MA, Friedrich MG, Ho VB, Jerosch-Herold M, Kramer CM, Manning WJ, Patel M, Pohost GM, Stillman AE, White RD, Woodard PK. ACCF/ACR/AHA/NASCI/SCMR 2010 expert consensus document on cardiovascular magnetic resonance: a report of the American College of Cardiology Foundation Task Force on Expert Consensus Documents. J Am Coll Cardiol. 2010; 55(23):2614–62. [PubMed: 20513610]
3. Barkhausen J, Goyen M, Ruhm SG, Eggebrecht H, Debatin JF, Ladd ME. Assessment of ventricular function with single breath-hold real-time steady-state free precession cine MR imaging. AJR Am J Roentgenol. 2002; 178(3):731–5. [PubMed: 11856708]
4. Kellman P, Chefd'hotel C, Lorenz CH, Mancini C, Arai AE, McVeigh ER. Fully automatic, retrospective enhancement of real-time acquired cardiac cine MR images using image-based navigators and respiratory motion-corrected averaging. Magn Reson Med. 2008; 59(4):771–8. [PubMed: 18302227]
5. Kellman P, Chefd'hotel C, Lorenz CH, Mancini C, Arai AE, McVeigh ER. High spatial and temporal resolution cardiac cine MRI from retrospective reconstruction of data acquired in real time using motion correction and resorting. Magn Reson Med. 2009; 62(6):1557–64. [PubMed: 19780155]
6. Christodoulou AG, Brinegar C, Haldar JP, Zhang H, Wu YJ, Foley LM, Hitchens T, Ye Q, Ho C, Liang ZP. High-resolution cardiac MRI using partially separable functions and weighted spatial smoothness regularization. Conf Proc IEEE Eng Med Biol Soc. 2010; 2010:871–4. [PubMed: 21097198]
7. Muthurangu V, Lurz P, Critchely JD, Deanfield JE, Taylor AM, Hansen MS. Real-time assessment of right and left ventricular volumes and function in patients with congenital heart disease by using high spatiotemporal resolution radial k-t SENSE. Radiology. 2008; 248(3):782–91. [PubMed: 18632528]
8. Seiberlich N, Ehses P, Duerk J, Gilkeson R, Griswold M. Improved radial GRAPPA calibration for real-time free-breathing cardiac imaging. Magn Reson Med. 2011; 65(2):492–505. [PubMed: 20872865]
9. Seiberlich N, Lee G, Ehses P, Duerk JL, Gilkeson R, Griswold M. Improved temporal resolution in cardiac imaging using through-time spiral GRAPPA. Magn Reson Med. 2011; 66(6):1682–8. [PubMed: 21523823]
10. Feng L, Srichai MB, Lim RP, Harrison A, King W, Adluru G, Dibella EV, Sodickson DK, Otazo R, Kim D. Highly accelerated real-time cardiac cine MRI using k-t SPARSE-SENSE. Magn Reson Med. 2013; 70(1):64–74. [PubMed: 22887290]
11. Kido T, Kido T, Nakamura M, Watanabe K, Schmidt M, Forman C, Mochizuki T. Compressed sensing real-time cine cardiovascular magnetic resonance: accurate assessment of left ventricular function in a single-breath-hold. J Cardiovasc Magn Reson. 2016; 18(1):50. [PubMed: 27553656]

12. Voit D, Zhang S, Unterberg-Buchwald C, Sohns JM, Lotz J, Frahm J. Real-time cardiovascular magnetic resonance at 1.5 T using balanced SSFP and 40 ms resolution. J Cardiovasc Magn Reson. 2013; 15:79. [PubMed: 24028285]
13. Goebel J, Nensa F, Schemuth HP, Maderwald S, Quick HH, Schlosser T, Nassenstein K. Real-time SPARSE-SENSE cine MR imaging in atrial fibrillation: a feasibility study. Acta Radiol. 2017; 58(8):922–8. [PubMed: 28273733]
14. Schaeffter T, Weiss S, Eggers H, Rasche V. Projection reconstruction balanced fast field echo for interactive real-time cardiac imaging. Magn Reson Med. 2001; 46(6):1238–41. [PubMed: 11746592]
15. Axel L, Sodickson DK. The Need for Speed: Accelerating CMR Imaging Assessment of Cardiac Function. JACC Cardiovasc Imaging. 2014; 7(9):893–5. [PubMed: 25212794]
16. Wundrak S, Paul J, Ulrici J, Hell E, Rasche V. A Small Surrogate for the Golden Angle in Time-Resolved Radial MRI Based on Generalized Fibonacci Sequences. IEEE Trans Med Imaging. 2015; 34(6):1262–9. [PubMed: 25532172]
17. Bieri O, Markl M, Scheffler K. Analysis and compensation of eddy currents in balanced SSFP. Magn Reson Med. 2005; 54(1):129–37. [PubMed: 15968648]
18. Wundrak S, Paul J, Ulrici J, Hell E, Geibel MA, Bernhardt P, Rottbauer W, Rasche V. Golden ratio sparse MRI using tiny golden angles. Magn Reson Med. 2016; 75(6):2372–8. [PubMed: 26148753]
19. Winkelmann S, Schaeffter T, Koehler T, Eggers H, Doessel O. An optimal radial profile order based on the Golden Ratio for time-resolved MRI. IEEE Trans Med Imaging. 2007; 26(1):68–76. [PubMed: 17243585]
20. Zhou W, Bovik AC, Sheikh HR, Simoncelli EP. Image quality assessment: from error visibility to structural similarity. IEEE Transactions on Image Processing. 2004; 13(4):600–12. [PubMed: 15376593]
21. Block, K., Uecker, M. Simple method for adaptive gradient-delay compensation in radial MRI. Proceedings of the 19rd Annual Meeting of ISMRM, Montreal; Quebec, Canada. 2011; Abstract No. 2816
22. Griswold MA, Jakob PM, Heidemann RM, Nittka M, Jellus V, Wang J, Kiefer B, Haase A. Generalized autocalibrating partially parallel acquisitions (GRAPPA). Magn Reson Med. 2002; 47(6):1202–10. [PubMed: 12111967]
23. Feng L, Grimm R, Block KT, Chandarana H, Kim S, Xu J, Axel L, Sodickson DK, Otazo R. Golden-angle radial sparse parallel MRI: combination of compressed sensing, parallel imaging, and golden-angle radial sampling for fast and flexible dynamic volumetric MRI. Magn Reson Med. 2014; 72(3):707–17. [PubMed: 24142845]
24. Dutt A, Rokhlin V. Fast Fourier-Transforms for Nonequispaced Data. Siam Journal on Scientific Computing. 1993; 14(6):1368–93.
25. Uecker M, Zhang S, Voit D, Karaus A, Merboldt KD, Frahm J. Real-time MRI at a resolution of 20 ms. NMR Biomed. 2010; 23(8):986–94. [PubMed: 20799371]
26. Xue H, Kellman P, Larocca G, Arai AE, Hansen MS. High spatial and temporal resolution retrospective cine cardiovascular magnetic resonance from shortened free breathing real-time acquisitions. J Cardiovasc Magn Reson. 2013; 15:102. [PubMed: 24228930]

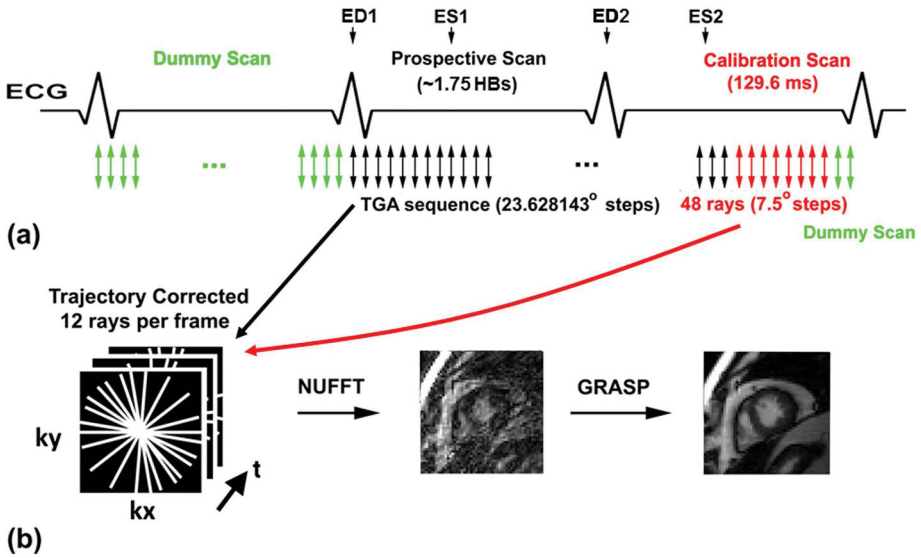

Figure 1.

(a) Pulse sequence diagram showing our sampling strategy. The first heartbeat was used to play pre-scan, dummy scans (green arrows) to approach steady state of magnetization. This is standard for all cine MRI with b-SSFP. Real-time, radial data were acquired in the subsequent 1.75 heartbeats using the TGA sequence (black arrows). Immediately after current data scan and before start of pre-scan, dummy scans for the following imaging plane, 48 rays of calibration data (red arrows; a pair of rays with opposite polarities per direction; 7.5° angular steps) were acquired in lieu of post-scan dummy scans (green arrows).

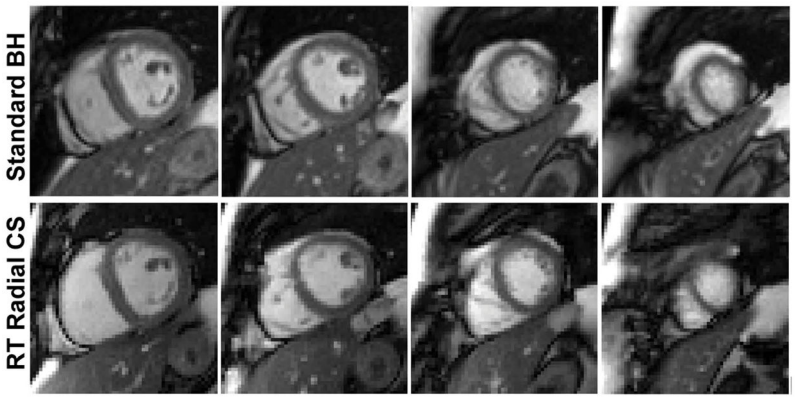

Figure 2.

Representative multi-slice cine images of a patient with MI acquired at 1.5T. Real-time cine with radial CS produced results that approximate those produced by standard cine MRI. For the corresponding movie files, see Supporting Information (Video S1.avi for standard cine, Video S2.avi for real-time with radial CS).

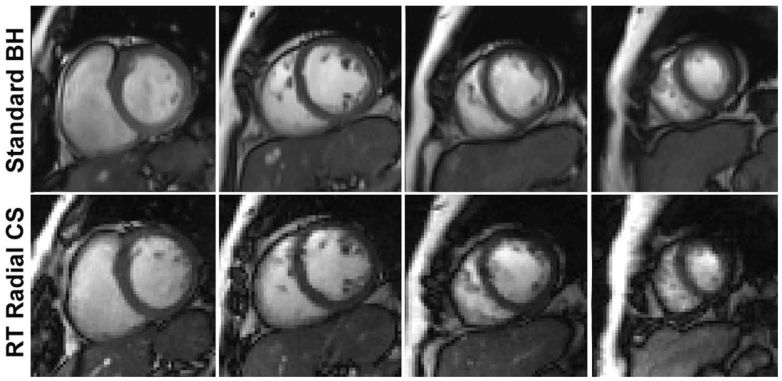

Figure 3.

Representative multi-slice cine images of a patient with CKD acquired at 3T. Real-time cine with radial CS produced results that approximate those produced by standard cine MRI. For the corresponding movie files, see Supporting Information (Video S3.avi for standard cine, Video S4.avi for real-time with radial CS).

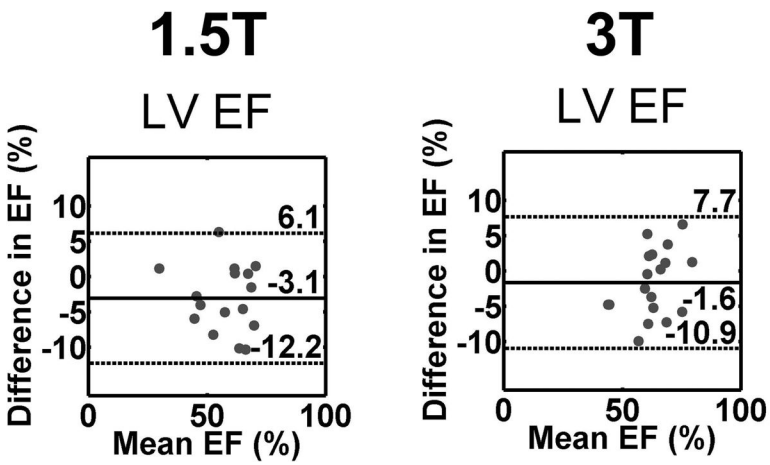

Figure 4.

The Bland-Altman plots showing agreement in LVEF between standard cine (reference) and real-time cine MRI pulse sequences: standard vs. real-time with radial CS at 1.5T (1st column), and standard vs. real-time with radial CS at 3T (second column). The mean difference in LVEF was −3.0 and −1.6% for 1.5T and 3T, respectively, which correspond to −5.3 and −2.6% error relative to mean LVEF values 57.9 and 63.2 % at 1.5T and 3T, respectively.

Table 1

A summary of averaged reader scores for each of four categories per pulse sequence per field strength. The two groups (standard and real-time with radial CS) were significantly different for temporal fidelity, artifact, and noise scores (P = 0.013), except for myocardial wall definition (P > 0.05). Interestingly, real-time cine with radial CS produced higher artifact and noise scores than standard cine. Each category is scored from 1 to 5 (worst to best). Note that for all four categories, mean scores were greater than 3.0, suggesting that all scores were deemed clinically usable by our readers.

Field Strength	Sequence	Myocardial Edge Definition	Temporal Fidelity	Artifact	Noise
1.5T (N=16)	***Standard Cine***	4.4 ± 0.5	4.9 ± 0.3*	4.2 ± 1.0*	4.4 ± 0.3*
	Radial CS	4.6 ± 0.4	4.4 ± 0.6*	4.8 ± 0.3*	4.8 ± 0.3*
3T (N=18)	***Standard Cine***	4.6 ± 0.6	5.0 ± 0.1*	4.3 ± 0.7*	5.0 ± 0.0
	Radial CS	4.5 ± 0.5	4.3 ± 0.6*	4.7 ± 0.3*	4.9 ± 0.2